Mott Metal-Insulator Transitions in Pressurized Layered Trichalcogenides

Heung-Sik Kim,[1,2] Kristjan Haule,[1] and David Vanderbilt[1]
[1]Department of Physics and Astronomy, Rutgers University, Piscataway, New Jersey 08854-8019, USA
[2]Department of Physics, Kangwon National University, Chuncheon 24341, Korea

(Received 27 August 2018; revised manuscript received 17 September 2019; published 3 December 2019)

Transition metal phosphorous trichalcogenides, MPX_3 (M and X being transition metal and chalcogen elements, respectively), have been the focus of substantial interest recently because they are unusual candidates undergoing Mott transition in the two-dimensional limit. Here we investigate material properties of the compounds with $M =$ Mn and Ni employing *ab initio* density functional and dynamical mean-field calculations, especially their electronic behavior under external pressure in the paramagnetic phase. Mott metal-insulator transitions (MIT) are found to be a common feature for both compounds, but their lattice structures show drastically different behaviors depending on the relevant orbital degrees of freedom, i.e., t_{2g} or e_g. Under pressure, $MnPS_3$ can undergo an isosymmetric structural transition within monoclinic space group by forming Mn-Mn dimers due to the strong direct overlap between the neighboring t_{2g} orbitals, accompanied by a significant volume collapse and a spin-state transition. In contrast, $NiPS_3$ and $NiPSe_3$, with their active e_g orbital degrees of freedom, do not show a structural change at the MIT pressure or deep in the metallic phase within the monoclinic symmetry. Hence $NiPS_3$ and $NiPSe_3$ become rare examples of materials hosting electronic bandwidth-controlled Mott MITs, thus showing promise for ultrafast resistivity switching behavior.

DOI: 10.1103/PhysRevLett.123.236401

Since the first identification of the Mott metal-insulator transition (MIT) by Mott and Peierls in 1937 [1] and the suggestion of the canonical Hubbard model in 1963 [2], many systems showing the Mott MIT have been found. They can be broadly classified into two categories, (i) the filling-controlled MITs, such as in the doped cuprates [3], or (ii) the bandwidth-controlled MITs, such as in the rare-earth nickelates $R\mathrm{NiO_3}$ (R being a rare-earth element) [4,5] or vanadium oxides V_2O_3 [6–8] and VO_2 [6,9]. Considering applications to electronic resistive switching devices, the filling-controlled MIT of type (i) is not favorable due to the inevitable strong inhomogeneity at the atomic scale introduced by the chemical doping. The bandwidth-controlled MITs of type (ii), on the other hand, are typically coupled strongly to the structural degrees of freedom, as for examples in the bond disproportionation between the short and long Ni-O bonds in $R\mathrm{NiO_3}$ [10–13] and the dimerization of vanadium atoms in VO_2 [14,15]. Such involvement of slow lattice dynamics in the MIT is also not favorable for fast switching. Hence, systems with *electronic* bandwidth-controlled MITs (i.e., weak or no lattice distortions involved) are desirable for fast resistive switching [16,17].

Surprisingly, there are very few solids that are known to undergo purely electronic and bandwidth-controlled MITs, as was originally envisioned by Hubbard. From the theoretical side, there is growing evidence that starting from the metallic side, the MIT would not have occurred in any of above three systems ($R\mathrm{NiO_3}$, V_2O_3, and VO_2) in the absence of a simultaneous structural distortion. Even less common are such transitions in two-dimensional materials, which might be useful for ultrathin electronic and spintronic applications, and to our knowledge there is no known example of an electronically driven MIT among the van der Waals (vdW) materials except the recently discovered Mott phase and superconductivity in twisted bilayer graphene [18,19].

Here we propose new candidates for the electronic bandwidth-controlled MIT without significant structural distortion among the emerging class of two-dimensional vdW materials. Our target is a series of transition metal phosphorous trichalcogenides MPX_3 ($M =$ Mn, Ni, $X =$ S, Se) [20–22]. To incorporate the electronic and structural degrees of freedom on an equal footing, we employ the state-of-the-art embedded dynamical mean-field theory combined with density functional theory (EDMFT), which implements forces on atoms and allows relaxation of internal atomic coordinates [23]. For the optimization of the size and shape of unit cells we use density functional theory (DFT) augmented by the on site Coulomb repulsion U (DFT + U), after which optimizations of internal atomic coordinates are performed both in EDMFT and DFT + U yielding consistent results [24]. We mainly focus on paramagnetic phases of $MnPS_3$ and $NiP\{S, Se\}_3$ above their Néel temperatures ($T_N = 78$ and 154 K for $MnPS_3$ and $NiPS_3$, respectively [31–33]), with disordered local Mn^{2+} (d^5) $S = 5/2$ and Ni^{2+} (d^8) $S = 1$ moments, although the behavior of their MITs in the magnetic phases is discussed

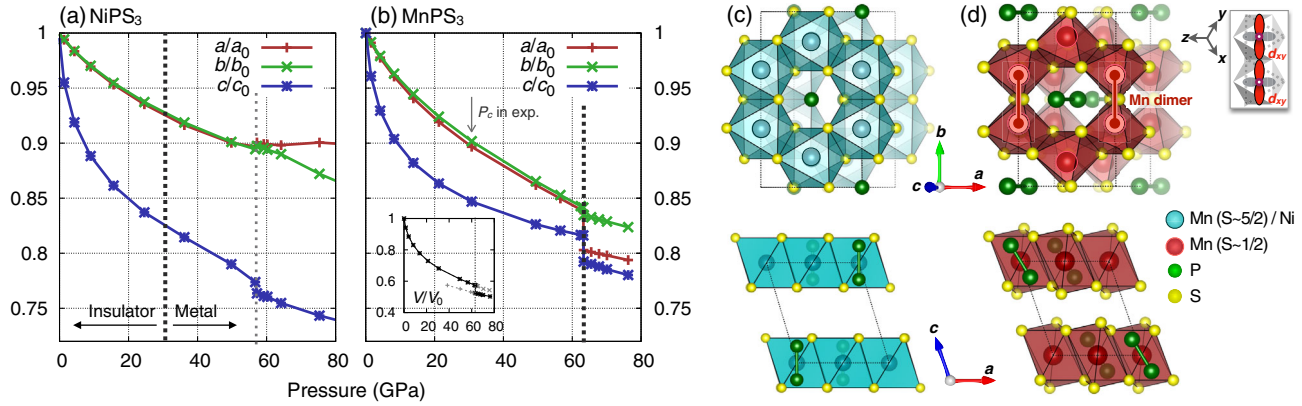

FIG. 1. (a), (b) Evolution of DFT + U-optimized lattice parameters [a, b, and c as depicted in (c), (d)] as a function of pressure, where (a) and (b) panels show results from $NiPS_3$ and $MnPS_3$, respectively. Inset in (b) shows a volume versus pressure plot for $MnPS_3$, where black and gray curves represent ground-state and metastable structures, respectively. Thick vertical dashed lines in both plots indicate the values of critical pressure where the MIT happens. The thin dotted line in (a) shows the pressure where the a/a_0 and b/b_0 begin to branch in $NiPS_3$ (i.e., $b \neq \sqrt{3}a$) due to the enhanced monoclinicity by pressure. Note that, the critical pressure for $MnPS_3$ reported in Ref. [20] is around 30 GPa, as depicted in the figure. (c) Crystal structures for $NiPS_3$ and $MnPS_3$ at the ambient pressure. (d) $MnPS_3$ structure when $P > 64$ GPa, where the Mn dimer is formed parallel to b.

in the Supplemental Material [28]. We will show that the recently discovered MIT in $MnPS_3$ falls under the family of transitions coupled to structural changes, in which the dimerization plays a crucial role, therefore bearing a resemblance to the MIT in VO_2 [20]. On the other hand, theoretical simulations in $NiPS_3$ and $NiPSe_3$ suggest that the MIT in these two vdW compounds occurs at even lower pressure, and does not involve a simultaneous structural transition. Therefore they become rare examples of electronic bandwidth-controlled transitions with a potential for very fast resistive switching.

Crystal structures versus pressure.—Figures 1(a) and 1(b) show DFT + U results on the pressure-induced change of the three lattice parameters (a/a_0, b/b_0, and c/c_0, where $\{a, b, c\}_0$ denote their zero-pressure values) for $NiPS_3$ and $MnPS_3$, respectively. Note that here we focus on the monoclinic $C2/m$ structure as shown in Fig. 1(c). Because both of the compounds are vdW-type layered systems, the interplane lattice parameter c shows a steeper decrease compared to the in plane a and b, and the threefold symmetry within each layer forces $b \simeq \sqrt{3}a$ in the low-P regime. The resulting volume decrease under pressure is substantial: 40% of volume reduction at ~50 GPa compared to the ambient pressure volume, as shown in the inset of Fig. 1(b).

Both compounds show MIT and structural phase transitions under pressure, but the nature of their transition is drastically different. As shown in Fig. 1(a), the MIT and the structural transition in $NiPS_3$ occur at very different pressures, around 31 and 57 GPa, respectively, while they coincide in $MnPS_3$. Remarkably, theoretical simulations suggest that the MIT in $NiPS_3$ accompanies no significant structural distortion (discontinuous structural changes, for example), and is thus a rare example of an electronically driven bandwidth-controlled MIT. On the other hand, in $MnPS_3$ the isosymmetric structural transition (i.e., structural transition within the same space group symmetry) with a volume collapse at 63 GPa is crucial for the occurrence of the MIT; hence the transition is better classified as the structurally assisted MIT [see Fig. 1(b)]. We note that the theoretical critical pressure of 63 GPa is somewhat overestimated compared to the experimentally reported value of ~30 GPa [20]. However, we show in the Supplemental Material [28] that within EDMFT, spinodal lines extend down to a much lower pressure of 40 GPa with a much reduced energy barrier between the metallic and insulating solutions compared to the DFT + U results. Inclusion of the phonon free energy and the lattice zero-point energy, which is neglected here, could then move the position of the transition significantly (see the Supplemental Material for further details).

In addition to the volume collapse, mostly from the discontinuous change of a, DFT + U simulations of $MnPS_3$ show a Mn-Mn dimerization along the b direction with the tilting of the P_2 dimer as shown in Fig. 1(d). The Mn-Mn bond lengths between the dimer and nondimer bonds are 2.42 and 3.10 Å at 63 GPa, respectively, which is a rather large difference. This Mn dimer formation is attributed to the direct d-d overlap between the Mn t_{2g} orbitals, pointing directly towards the nearest-neighbor Mn as shown in the inset of Fig. 1(d). Note that the previous experimental study suggested the formation of Mn zigzag chains in the high-P phase [20], in contrast to our DFT + U and EDMFT results.

$NiPS_3$, on the other hand, shows no such intermetallic dimerization or chain formation at the MIT or beyond the structural transition pressure, because the partially filled Ni e_g orbitals point towards the S atoms. This makes $NiPS_3$ more sensitive to the p-d hybridization, yielding a smaller

MIT pressure in $NiPS_3$ compared to $MnPS_3$. Such a stark contrast between $NiPS_3$ and $MnPS_3$, originating from the difference in their orbital physics, affects the nature of the structural behavior of their MIT as shown below. Note that the structural transition in $NiPS_3$ at 57 GPa is not orbital in nature and comes purely from the reduced interlayer distance and the large overlap between the layers.

We note that the two compounds show markedly different pressure dependence of the lattice parameters even before the structural transition. By comparing Figs. 1(a) and 1(b) it is evident that the compression of c under pressure is stronger in $NiPS_3$ than in $MnPS_3$; while $a/a_0 - c/c_0$ in $MnPS_3$ at 60 GPa is about 0.03 [see Fig. 1(b)], in $NiPS_3$ it is about 0.15 [Fig. 1(a)] despite the similar volume change. In other words, it is much easier to compress $NiPS_3$ along the layer-normal direction compared to $MnPS_3$. Because the kinetic energy scale set by the hopping integrals between the t_{2g} (for $MnPS_3$) and e_g (for $NiPS_3$) orbitals show different anisotropy, the t_{2g} and e_g yield strong in plane d-d and interplane d-p-p-d overlaps, respectively (see the Supplemental Material [28]). As a result, while the t_{2g} orbitals favor in plane compression for the larger in plane kinetic energy gain, the e_g orbitals prefer to reduce the interplane distance, yielding the tendency shown in Figs. 1(a) and 1(b).

Electronic MIT in $NiPS_3$.—Below we take a closer look into the nature of the MIT in $NiPS_3$. Note that all the spectra presented hereafter are EDMFT results, where the (DFT + U)-optimized cell parameters and estimated pressure values are employed. Figure 2(a) shows projected densities of states (PDOS) of $NiPS_3$ with varying pressure from 0 to 88 GPa. It is clear that the t_{2g} states (a_g and e'_g) are mostly occupied, while the e_g states are partially filled and show a narrow dip at the Fermi level at 30.4 GPa. The self-energies of the e_g orbitals show poles at the Fermi level (see the Supplemental Material [28]), confirming the presence of the paramagnetic Mott phase. Previously, it was suggested that $NiPS_3$ is a negative charge-transfer (NCT) insulator with a $d^9\underline{L}^1$ configuration ($\underline{L}$ denoting a S p-ligand hole) [21]. However, our EDMFT results show that when the Ni occupation is close to $n_d \approx 9$, where the $d^9\underline{L}^1$ configuration is dominant, the Mott insulating state cannot be stabilized; i.e., the material is metallic. The experimentally observed Mott insulating behavior can only be achieved with the Ni occupancy of $n_d \approx 8$, where the high-spin $S = 1$ configuration is dominant, i.e., corresponding to approximately half-filled e_g states [see Fig. 2(b) for the probability distribution in the insulating and metallic states]. This observation is corroborated by x-ray absorption spectroscopy, indicating that $NiPS_3$ is close to the NCT regime, but is still dominated by the d^8 $S = 1$ configuration, consistent with our EDMFT results [34].

Figure 2(b) shows the valence histogram for the few most important Ni d configurations versus pressure at

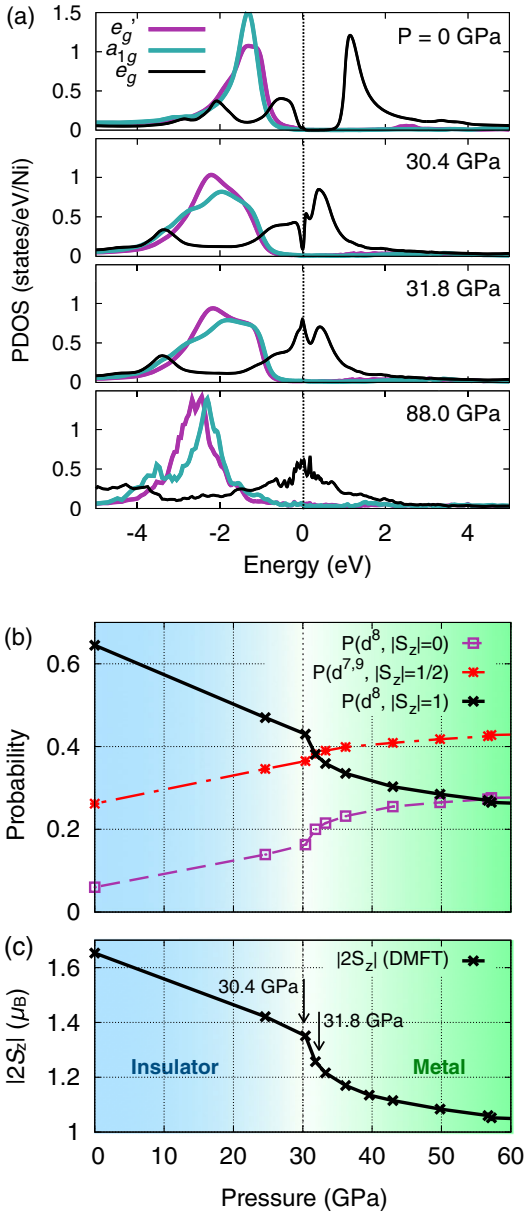

FIG. 2. (a) Projected density of states (PDOS) in the paramagnetic phase of $NiPS_3$ at $T = 232$ K, calculated by EDMFT with the increasing pressure from the ambient condition (top panel) to 88 GPa (lowest). (b) Monte Carlo probabilities for the d^8 $|S_z| = 0$ (purple dashed line), $d^{7,9}$ $|S_z| = 1/2$ (red dash dotted), and d^8 $|S_z| = 1$ (black solid) as a function of pressure. (c) Pressure dependence of the size of PM Ni spin moment $|2S_z|$ from PM EDMFT results at $T = 232$ K. Note a cusp at $P = 30.4$ GPa where the MIT happens.

$T = 232$ K. The Mott insulating state is stable as long as the high-spin state ($|S_z| = 1$) of the Ni-d^8 configuration is dominant. Note that we report S_z values rather than S values, because of our choice of an Ising-type approximation of the Coulomb interaction in the EDMFT impurity solver [35]. Around 31 GPa the $|S_z| = 1/2$ states (of d^9 and d^7 configurations) become equally probable, at which point

the Mott state collapses and a narrow metallic quasiparticle peak appears [see the third panel in Fig. 2(a)]. Despite the enhanced charge fluctuation, the change of Ni d-orbital occupation (n_d) across the transition is negligible: $n_d = 8.15$ and 8.19 at $P = 0$ and 88 GPa, respectively. The increase of charge fluctuations with increasing pressure has an additional effect of unlocking the $|S_z| = 0$ sector of the d^8 configuration, which is favored in the itinerant low spin regime at large pressure. Note that the increase of the probability for $|S_z| = 0$ at the expense of the $|S_z| = 1$ state has a large effect on the size of the fluctuating moment $|2S_z|$, which is plotted in Fig. 2(c). Its zero-pressure value is around $1.6\mu_B$, which is quite reduced from the maximum atomic value of $2\mu_B$, and once it is reduced below $1.4\mu_B$ it drops very suddenly and takes values of $\lesssim 1.3\mu_B$ in the metallic state. We note that the change between 30.4 and 31.8 GPa is abrupt, which is likely associated with a first-order transition, for which a coexistence of both solutions is expected. However the hysteresis was not observed, probably because it is too narrow at the temperature studied ($T = 232$ K). We mention that the MIT was carefully checked by employing beyond-Ising Coulomb interaction terms (spin-flip and pair-hopping types) at a lower temperature of $T = 116$ K, but neither a hysteretic behavior nor a discontinuity in the energy-volume curve were found, signifying very weak coupling between the lattice and charge degrees of freedom in $NiPS_3$ (see Sec. III. A in the Supplemental Material [28] and Fig. S3 therein for more details).

MIT driven by uniaxial pressure in $NiPSe_3$.—While the critical pressure for the MIT in $NiPS_3$ can be reached in modern high-pressure experimental setups, a substitution of S by the more polarizable Se is expected to further reduce the critical pressure. Therefore the recently synthesized $NiPSe_3$ [36] can be a better candidate for realizing the pressure-driven MIT compared to $NiPS_3$. Moreover, the collapse of the interlayer distance is expected to be sufficient to induce the MIT, which can even be achieved by the tip of an atomic-force microscope [37]. As a zeroth-order approximation, we simulate such layer-normal strain by varying the interlayer distance with fixed in plane lattice parameters, and allowing the internal coordinates to relax within EDMFT. In Fig. 3 we show the e_g PDOS of $NiPSe_3$ where the MIT happens at the modest stress of $13 \lesssim \sigma_z \lesssim 15$ GPa at $T = 58$ K, suggesting $NiPSe_3$ as another promising electronic bandwidth-controlled Mott transition system among these layered vdW materials.

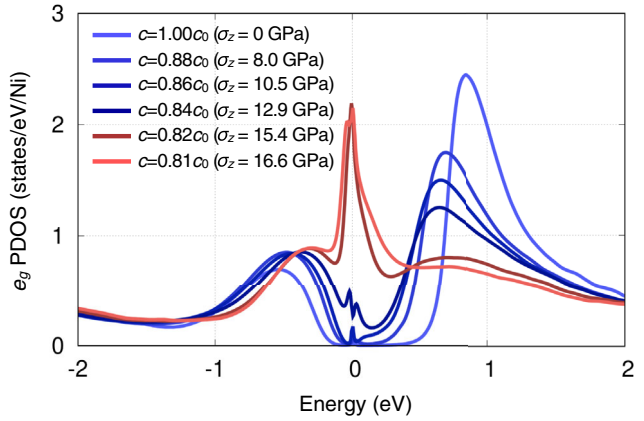

FIG. 3. $NiPSe_3$ e_g PDOS in the presence of an uniaxial stress σ_z along the layer-normal $\hat{z}$ direction from PM EDMFT results at $T = 58$ K (with varying σ_z from 0 to 16.6 GPa). Blue and red curves are PDOS for insulating and metallic phases, respectively, when the MIT happens between $\sigma_z = 15.4$ and 16.6 GPa.

Volume collapse and MIT in $MnPS_3$.—We now address the volume-collapse transition in $MnPS_3$. We first checked that once the optimized lattice parameters from DFT + U are employed, both DFT + U and EDMFT optimizations for the internal coordinates yield practically the same result.

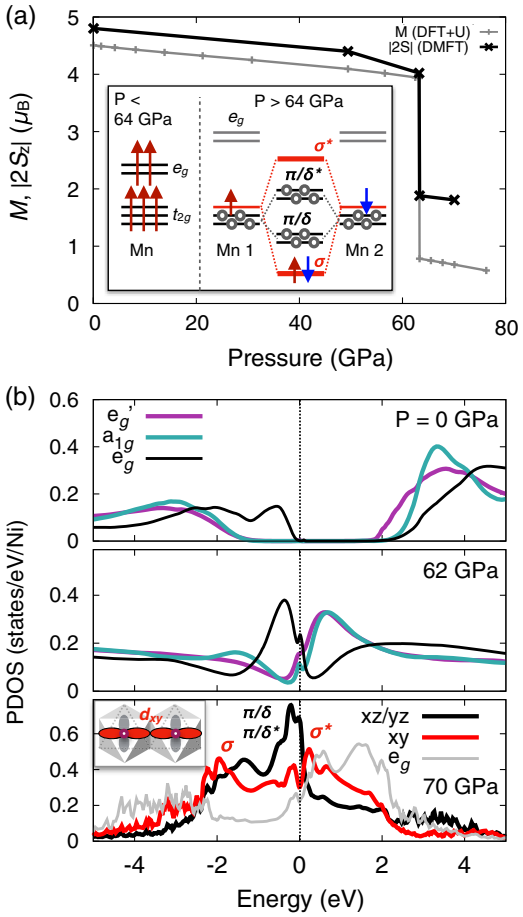

FIG. 4. (a) Pressure dependence of the size of Mn spin moment M from DFT + U (gray line) and $|2S_z|$ from paramagnetic EDMFT at $T = 580$ K (black), where both results show the spin-state transition at 63 GPa. The schematic spin-orbital configurations below and above the transition are shown in the inset. (b) PDOS from EDMFT, at $P = 0$ GPa (upper panel), 62 GPa (center), and 70 GPa (lower). Note that the choice of d orbital onto which the DOS are projected is different below and above the transition (e_g' and a_{1g} below, and $d_{xz,yz,xy}$ above 63 GPa).

Figure 4(a) shows the evolution of the fluctuating Mn moment $|2S_z|$ within the PM EDMFT at $T = 580$ K. We also show the ordered magnetic moment M (per Mn) within DFT + U in the Néel-type antiferromagnetic ordered state [20,31,38] (grey line in the plot). Perhaps not surprisingly, the two methods show very similar behavior: an insulating state of almost maximum spin $S = 5/2$ configuration in the low-to-intermediate-P regime, and a metallic state with strongly reduced Mn moments above $P = 64$ GPa. The inset of Fig. 4(a) schematically depicts the spin-orbital configuration below and above the transition. In the presence of strong external pressure, the orbitally inert high-spin $S = 5/2$ configuration becomes energetically unstable, and the low-spin $S = 1/2$ with the partially filled t_{2g} orbital is stabilized with an octahedral volume collapse [39]. As a result, the t_{2g} open shell in this edge-sharing geometry leads to a strong σ-like direct d-d overlap between the nearest-neighboring (NN) Mn sites, resulting in a strong tendency toward Mn dimerization [40]. At ambient pressure, because of the weak interlayer coupling, the three in plane NN bonds are essentially equivalent to each other. In the high-pressure regime, however, the monoclinicity originating from the layer stacking is no longer negligible. Therefore, the NN bond parallel to the b direction, which becomes nonequivalent to the other bonds, dimerizes as shown in Fig. 1(d) (see Sec. III. B in the Supplemental Material [28] for more details on inclusion of the beyond-Ising Coulomb terms).

Summary.—We report a theoretical study of the Mott MIT induced by external pressure in strongly correlated layered vdW materials. We comment that the Mott phases in other metal trisulfides, such as $FePS_3$ [41] or $CoPS_3$ [42], are also of great interest because of their partially filled t_{2g} shells even under ambient conditions. Overall, this family of vdW-layered transition metal trichalcogenides can be an excellent platform for the study of strong electron correlations and their cooperation with spin and lattice degrees of freedom.

We thank Matthew J. Coak, Michael O. Yokosuk, Nathan C. Harms, Kevin A. Smith, Sabine N. Neal, Janice L. Musfeldt, and Sang-Wook Cheong for helpful discussions. The work was supported by NSF DMREF Grant No. DMR-1629059. H. S. K. thanks the support of the research grant for new faculty members from Kangwon National University, and also the support of supercomputing resources including technical assistances from the National Supercomputing Center of Korea (Grant No. KSC-2019-CRE-0036)

[1] N. F. Mott and R. Peierls, Proc. Phys. Soc. **49**, 72 (1937).
[2] J. Hubbard, Proc. R. Soc. A **276**, 238 (1963).
[3] J. G. Bednorz and K. A. Müller, Z. Phys. B **64**, 189 (1986).
[4] J. B. Torrance, P. Lacorre, A. I. Nazzal, E. J. Ansaldo, and C. Niedermayer, Phys. Rev. B **45**, 8209 (1992).
[5] M. L. Medarde, J. Phys. Condens. Matter **9**, 1679 (1997).
[6] F. J. Morin, Phys. Rev. Lett. **3**, 34 (1959).
[7] D. B. McWhan, J. P. Remeika, T. M. Rice, W. F. Brinkman, J. P. Maita, and A. Menth, Phys. Rev. Lett. **27**, 941 (1971).
[8] S. A. Carter, T. F. Rosenbaum, P. Metcalf, J. M. Honig, and J. Spalek, Phys. Rev. B **48**, 16841 (1993).
[9] M. M. Qazilbash, M. Brehm, B.-G. Chae, P.-C. Ho, G. O. Andreev, B.-J. Kim, S. J. Yun, A. V. Balatsky, M. B. Maple, F. Keilmann, H.-T. Kim, and D. N. Basov, Science **318**, 1750 (2007).
[10] K. Haule and G. L. Pascut, Sci. Rep. **7**, 10375 (2017).
[11] S. Johnston, A. Mukherjee, I. Elfimov, M. Berciu, and G. A. Sawatzky, Phys. Rev. Lett. **112**, 106404 (2014).
[12] H. Park, A. J. Millis, and C. A. Marianetti, Phys. Rev. Lett. **109**, 156402 (2012).
[13] T. Mizokawa, D. I. Khomskii, and G. A. Sawatzky, Phys. Rev. B **61**, 11263 (2000).
[14] W. H. Brito, M. C. O. Aguiar, K. Haule, and G. Kotliar, Phys. Rev. Lett. **117**, 056402 (2016).
[15] S. Biermann, A. Poteryaev, A. I. Lichtenstein, and A. Georges, Phys. Rev. Lett. **94**, 026404 (2005).
[16] D. Ruzmetov, G. Gopalakrishnan, C. Ko, V. Narayanamurti, and S. Ramanathan, J. Appl. Phys. **107**, 114516 (2010).
[17] Z. Yang, C. Ko, and S. Ramanathan, Annu. Rev. Mater. Res. **41**, 337 (2011).
[18] Y. Cao, V. Fatemi, A. Demir, S. Fang, S. L. Tomarken, J. Y. Luo, J. D. Sanchez-Yamagishi, K. Watanabe, T. Taniguchi, E. Kaxiras, R. C. Ashoori, and P. Jarillo-Herrero, Nature (London) **556**, 80 (2018).
[19] Y. Cao, V. Fatemi, S. Fang, K. Watanabe, T. Taniguchi, E. Kaxiras, and P. Jarillo-Herrero, Nature (London) **556**, 43 (2018).
[20] Y. Wang, Z. Zhou, T. Wen, Y. Zhou, N. Li, F. Han, Y. Xiao, P. Chow, J. Sun, M. Pravica, A. L. Cornelius, W. Yang, and Y. Zhao, J. Am. Chem. Soc. **138**, 15751 (2016).
[21] S. Y. Kim, T. Y. Kim, L. J. Sandilands, S. Sinn, M.-C. Lee, J. Son, S. Lee, K.-Y. Choi, W. Kim, B.-G. Park, C. Jeon, H.-D. Kim, C.-H. Park, J.-G. Park, S. J. Moon, and T. W. Noh, Phys. Rev. Lett. **120**, 136402 (2018).
[22] J.-G. Park, J. Phys. Condens. Matter **28**, 301001 (2016).
[23] K. Haule, J. Phys. Soc. Jpn. **87**, 041005 (2018).
[24] For DFT + DMFT calculations we use the Rutgers DFT + Embedded DMFT code [25], while for DFT and DFT + U calculation we used the Vienna *ab initio* Simulation Package [26,27]. Dependency to different choices of exchange-correlation functionals, including van der Waals functionals, was also checked. Computational details are provided in the Supplemental Material [28], where we discuss the difference between the U values employed in our EDMFT calculations and other studies [29,30].
[25] K. Haule, C.-H. Yee, and K. Kim, Phys. Rev. B **81**, 195107 (2010).
[26] G. Kresse and J. Hafner, Phys. Rev. B **47**, 558 (1993).
[27] G. Kresse and J. Furthmüller, Phys. Rev. B **54**, 11169 (1996).
[28] See the Supplemental Material at http://link.aps.org/supplemental/10.1103/PhysRevLett.123.236401 for computational details.
[29] K. Haule, T. Birol, and G. Kotliar, Phys. Rev. B **90**, 075136 (2014).
[30] S. Mandal, K. Haule, K. M. Rabe, and D. Vanderbilt, arXiv:1907.10498.

[31] R. Brec, Solid State Ionics **22**, 3 (1986).
[32] A. R. Wildes, H. M. Rønnow, B. Roessli, M. J. Harris, and K. W. Godfrey, Phys. Rev. B **74**, 094422 (2006).
[33] A. R. Wildes, V. Simonet, E. Ressouche, G. J. McIntyre, M. Avdeev, E. Suard, S. A. J. Kimber, D. Lançon, G. Pepe, B. Moubaraki, and T. J. Hicks, Phys. Rev. B **92**, 224408 (2015).
[34] B. Pal, H.-S. Kim, K. Haule, D. Vanderbilt, J. Chakhalian, and J. Freeland (to be published).
[35] This approximation leads to some mixing between $S = 0$ and 1 states, but is not expected to change qualitative aspects of the results.
[36] J.-Q. Yan, B. C. Sales, M. A. Susner, and M. A. McGuire, Phys. Rev. Mater. **1**, 023402 (2017).
[37] H. Lu, C.-W. Bark, D. Esque de los Ojos, J. Alcala, C. B. Eom, G. Catalan, and A. Gruverman, Science **336**, 59 (2012).
[38] K. Okuda, K. Kurosawa, S. Saito, M. Honda, Z. Yu, and M. Date, J. Phys. Soc. Jpn. **55**, 4456 (1986).
[39] J. Kuneš, A. V. Lukoyanov, V. I. Anisimov, R. T. Scalettar, and W. E. Pickett, Nat. Mater. **7**, 198 (2008).
[40] S. V. Streltsov and D. I. Khomskii, Proc. Natl. Acad. Sci. U.S.A. **113**, 10491 (2016).
[41] J.-U. Lee, S. Lee, J. H. Ryoo, S. Kang, T. Y. Kim, P. Kim, C.-H. Park, J.-G. Park, and H. Cheong, Nano Lett. **16**, 7433 (2016).
[42] A. R. Wildes, V. Simonet, E. Ressouche, R. Ballou, and G. J. McIntyre, J. Phys. Condens. Matter **29**, 455801 (2017).